WITHDRAWAL OF PAIRS OF THREADED RODS WITH SMALL EDGE DISTANCES AND SPACINGS

Haris Stamatopoulos[1*] and Kjell Arne Malo[1]

[1]Department of Structural Engineering, Norwegian University of Science and Technology (NTNU), Rich. Birkelandsvei 1A, 7491, Trondheim, Norway.

* Corresponding author, Tel: +47 735 94675, Email: haris.stamatopoulos@ntnu.no

ABSTRACT: An experimental investigation on withdrawal of pairs of screwed-in threaded rods embedded in glued-laminated timber elements is presented in this paper. Specimens with varying angles between the rod axis and the grain direction (α= 15, 30, 60, 90°) and 2 different configurations with respect to edge distances and spacings were tested. The diameter and the embedment length of the rods were 20 mm and 450 mm, respectively. The threaded rods were embedded in a row perpendicular to the plain of the grain. The edge distances and spacings were smaller than the minimum requirements according to Eurocode 5. The withdrawal capacity of pairs of rods was compared to the withdrawal capacity of single rods and the effective number, n_{ef}, was found to be in the range 1.72-1.94, despite the small edge distances and spacings. Based on the obtained experimental results, a simple approximating expression was derived for n_{ef}. An analytical model based on Volkersen theory with an idealized bi-linear constitutive relationship was used to estimate the withdrawal capacity and stiffness. The analytical estimations were in good agreement with the experimental results. Finally, the withdrawal stiffness was estimated by use of finite element simulations. The numerical estimations for the withdrawal stiffness were also in good agreement with the experimental results.

KEYWORDS: Threaded rod, withdrawal, edge distance, spacing, rod-to-grain angle

1 INTRODUCTION

1.1 BACKGROUND

A remarkable increased use of axially loaded self-tapping screws and threaded rods, either as reinforcements or as fasteners in timber structures, has taken place in recent years. Threaded rods show in general high withdrawal capacity and stiffness, and thus they may be used to develop strong and stiff connections. In many practical cases multiple axially loaded threaded rods are used. Studies (Blaß and Laskewitz 1999; Gehri 2009; Krenn and Schickhofer 2009; Mahlknecht et al. 2014; Mori et al. 2008) have shown that connections with multiple axially loaded screws or glued-in rods can be very efficient, as each rod can reach a capacity in the order of 80-100% of the capacity of the respective single rod case. These studies have mainly focused on cases where the screws/rods were placed parallel or perpendicular to the grain direction. The background given in this Section is focusing on solid timber and glued-laminated timber (abbr. glulam).

The effectiveness of connections with multiple axially-loaded fasteners may be influenced by insufficient edge and end distances or spacings, as failure modes other than withdrawal or steel failure may be triggered and the full tensile capacity may not be reached. In order to take this into account, modern design codes and technical approvals set restrictions on the minimum edge and end distances as well as spacings. Typically, the minimum edge and end distances and spacings are provided as multiple of the outer thread diameter *d*. The minimum edge and end distances and spacings for screws according to EN1995 (abbr. EC5) (CEN 2004) are provided in Table 1. The associated definitions are specified in Fig. 1. As shown in Fig. 1, screws may be installed in rows parallel to the plane of the grain and thus sharing the same plane of the grain (for example screws 1-3-5 and 2-4-6) or in rows perpendicular to the plane of the grain and thus placed in different grain planes (for example screws 1-2, 3-4 and 5-6). For shortness, the former configuration is denoted as 'in-series' and the latter as 'in-parallel', confer Fig. 1.

Table 1: Minimum edge and end distances and spacings for screws according to EC5 (CEN 2004)

a_1	$7d$
$a_{1.CG}$	$10d$
a_2	$5d$
$a_{2.CG}$	$4d$

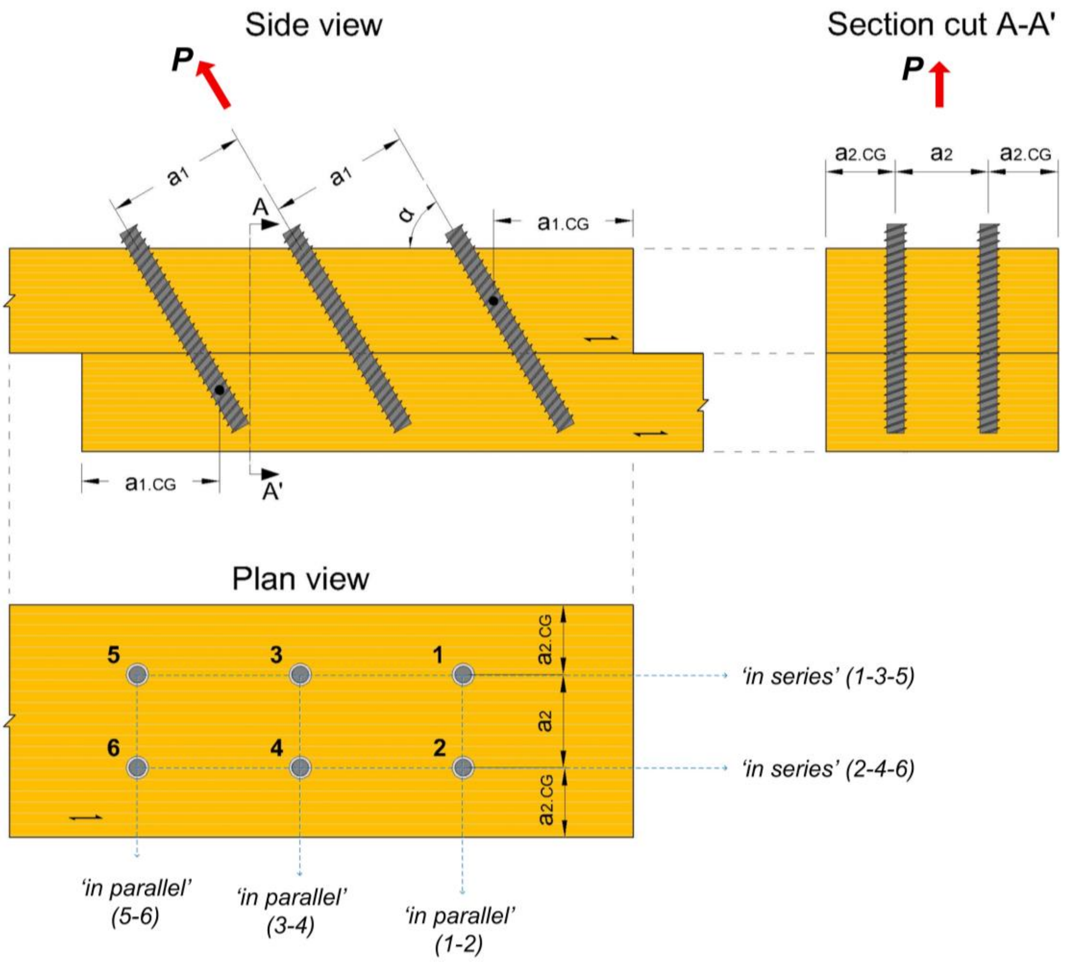

Fig. 1 Definitions of edge and end distances and spacings according to EC5 (CEN 2004) and naming of configurations

Small spacings (a_1, a_2) may lead to block/plug shear failures. Mahlknecht et al (2014) have shown that block shear failure may occur even if the minimum requirements given in Table 1 are fulfilled. For screws inserted parallel to the grain, small edge distances may lead to splitting failure (Nakatani and Walford 2010). Insertion of screws parallel to the grain without some sort of reinforcement against splitting should be avoided, because tensile stresses perpendicular to the grain may develop due to other reasons than withdrawal (for example moisture-induced stresses (Angst and Malo 2012)). In order to eliminate the risk of splitting, EC5 (CEN 2004) imposes the minimum edge and end distances of Table 1 and it does not allow for installation of screws in an angle to the grain direction less than 30°. According to DIN 1052:2008-12 (DIN 2008), the insertion of screws in pre-drilled holes has a positive effect in comparison to self-tapping screws and thus the minimum requirements for edge distances and spacings are less strict. However, this positive effect of pre-drilling is not taken into account in EC5 (CEN 2004).

According to EC5 (CEN 2004), the withdrawal capacity of connections with multiple axially loaded screws (which comply with the requirements in Table 1) is determined by multiplying the corresponding capacity of a single screw with the effective number of screws, n_{ef}, given by:

$$n_{ef} = n^{0.9} \tag{1}$$

where n is the number of screws acting together in a connection. The background research for Eq.(1) could not be located by the present authors. According to recent studies (Krenn and Schickhofer 2009; Mahlknecht et al. 2014), the effective number of screws is equal to the actual number with respect to withdrawal capacity (i.e. $n_{ef}= n$) for configurations where the requirements of Table 1 are fulfilled (and therefore Eq. (1) is conservative according to these studies).

EC5 (CEN 2004) does not provide guidelines for the estimation of withdrawal stiffness of axially loaded self-tapping screws or threaded rods. In the case of single self-tapping screws with diameters up to 12-14 mm, most research effort has been devoted on the determination of the withdrawal strength and the influence of several parameters on the withdrawal strength. Fewer results are available for the withdrawal stiffness. Some simple expressions for the withdrawal stiffness can be found in several technical approvals, see for example Z-9.1-472 (DIBt 2011) or ETA-11/0190 (DIBt 2013). However, the expressions found in these technical approvals: a) are different with respect to the effect of the diameter and the embedment length (possibly due to different experimental configurations), b) they do not take into account the influence of the angle between the screw and the grain direction and c) they cannot be extrapolated for threaded rods with greater dimeters (Stamatopoulos 2016). A proposal for the withdrawal stiffness of single axially loaded self-tapping screws based on a more systematic approach and a huge sample of experimental results can be found in (Ringhofer et al. 2015). In the case of multiple axially-loaded self-tapping screws the existing results for the withdrawal stiffness are sparse. Krenn and Schickhofer (2009), based on experimental results of axially loaded joints with inclined self-tapping screws and steel plates as outer members, have proposed the following effective number of screws for design in the serviceability limit state:

$$n_{ef.ser} = n^{0.8} \quad (2)$$

To the knowledge of the authors, there are no guidelines available for the withdrawal stiffness of single threaded rods with greater diameters in the present European technical approvals. Experimental results covering both withdrawal capacity and stiffness can be found in (Nakatani and Komatsu 2004) for rods with varying embedment length embedded parallel to the grain and in (Blaß and Krüger 2010) for rods with varying embedment length and diameter embedded with an angle of 45° and 90° to the grain direction. Another investigation on the withdrawal stiffness of single threaded rods with varying embedment lengths (l= 100, 300, 450, 600 mm) and rod-to-grain angles (α= 0, 10, 20, 30, 60 and 90°) by use of experimental, numerical and analytical methods has recently been presented by the present authors (Stamatopoulos and Malo 2016). The corresponding results with respect to the withdrawal capacity are given in (Stamatopoulos and Malo 2015a; Stamatopoulos and Malo 2015b).

In the case of multiple axially loaded threaded rods, the available experimental results are very sparse. (Mori et al. 2008) presented an experimental study of configurations with 1, 2 and 4 rods with varying spacing embedded parallel and perpendicular to the grain in glulam elements. According to this investigation, the full withdrawal capacity could be reached for spacing equal to 4 times the diameter whereas 80%-90% of the withdrawal capacity of a single rod was reached for specimens with spacing equal to 2 times the diameter. Similar results have been obtained by (Gehri 2009) in an investigation of the influence of spacing on withdrawal strength of self-tapping screws with a diameter of 10 mm embedded parallel to the grain (in this case the threshold spacing to reach the full withdrawal capacity was 5 times the diameter). With respect to withdrawal stiffness, (Mori et al. 2008) could not reach definite conclusions with respect to the withdrawal stiffness of multiple threaded rods.

1.2 OUTLINE

For a pair of threaded rods installed ‘in parallel’ in a timber element, the minimum required width is equal to 13d if the requirements of Table 1 are fulfilled. In practice however it may be desirable to install the rods with smaller edge distances and spacings. In the present study, only configurations with a pair of threaded rods installed in ‘parallel’ were investigated. In this configuration, plug shear failure cannot occur because shear stresses are concentrated towards the plane of the grain and the rods are embedded in different planes. On the contrary, in ‘series’ configurations with long, axially-loaded fasteners installed with small spacings are prone to plug shear failure because the fasteners share the same plane of the grain. The difference in the failure mode of the two configurations is illustrated in Fig. 2. Fig. 2a is taken from the present study and Fig. 2b is taken from a study on screws’ withdrawal from laminated veneer lumber elements (Carradine et al. 2009).

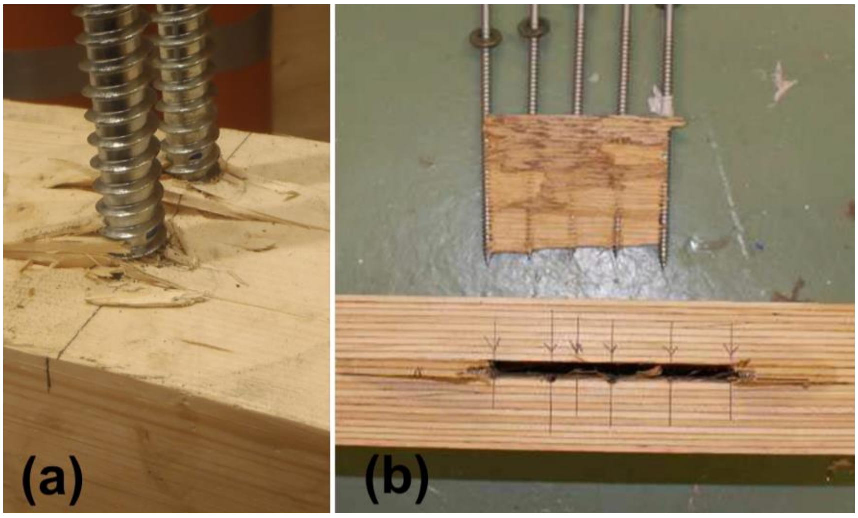

Fig. 2 Failure modes of configurations with small spacings: (a) 'in parallel' configuration, (b) 'in series' configuration (Carradine et al. 2009)

For long rods inserted with an inclination to the grain direction a splitting crack may form along the grain if the distance to the edge $a_{2.CG}$ is small. However, failure due to this crack may be prevented because the crack is bridged by the rod itself and any additional reinforcement against splitting which may exist. In the present study, the withdrawal of pairs of screwed-in threaded rods installed in 'parallel' with edge distances and spacings which do not comply with the minimum requirements of EC5 (CEN 2004) is investigated. Experimental, analytical and numerical methods are used.

2 MATERIALS AND METHODS

2.1 EXPERIMENTAL

The experimental set-up used for the withdrawal tests is presented in Fig. 3. The loading condition of the specimens was a 'remote' pull-push (i.e. the support was provided in the same plane surface as the entrance of the rods, but at a distance to the rods). The distance between the supports was s = 185 mm. A thin steel plate, as shown in Fig. 3d, was placed between the supports and the specimen in order to counteract tensile stresses due to bending, while allowing for local deformation on the surface of the specimen. The relative displacement between the rods and the supports was measured by two displacement transducers, attached to a steel apparatus clamped on the rods, as shown in Fig. 3f. The average of these two measurements was used for the displacement. To ensure equal deformation of the rods a very stiff coupling part was used, confer Fig. 3g.

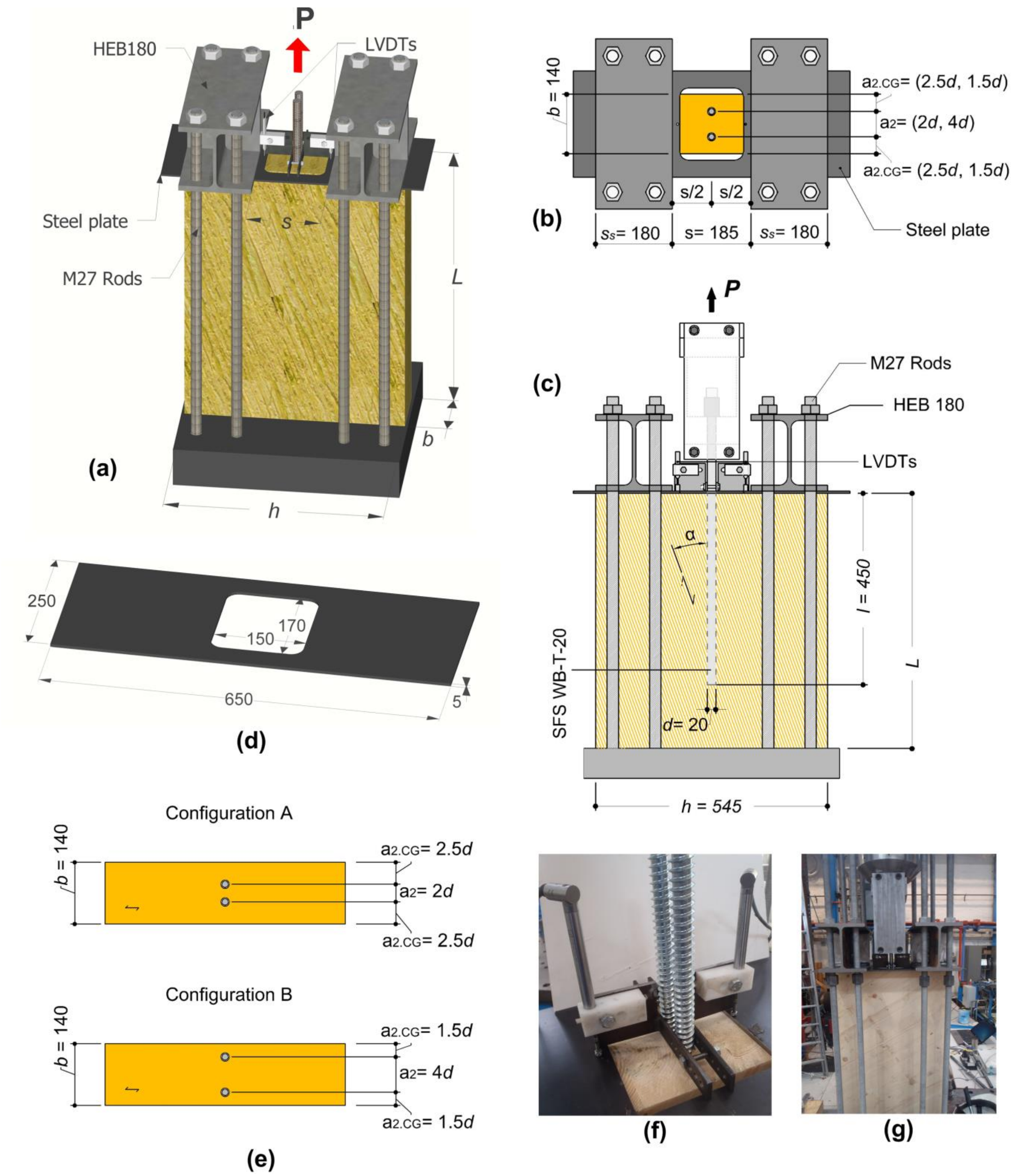

Fig. 3 Experimental set-up: (a) virtual 3D representation, (b) top view, (c) side view, (d) steel plate, (e) configurations A and B, (f) attachment of LVDTs and (g) photo

The specimens were cut from several glulam beams of Scandinavian class L40c which is a combined type of glulam corresponding to the European strength class GL30c (CEN 2013). This type of glulam is fabricated with 45 mm thick lamellas, made of Norwegian spruce (*Picea Abies*). Its mean and characteristic density are ρ_m= 470 kg/m^3 and ρ_k= 400 kg/m^3, respectively. For increased homogeneity, all specimens were manufactured such that the rods were embedded in the inner, weaker lamellas of the beams. Moreover, specimens were cut in such a way so that the rods were embedded in different laminations within the same specimen series. The width, *b*, of the glulam beams and consequently of all specimens was equal to 140 mm. SFS WB-T-20 (DIBt 2010) steel threaded rods were used. The outer-thread diameter, d, of the rods was 20 mm and the core diameter, d_c, was 15 mm. Prior to screwing-in of rods, all specimens were pre-drilled with a diameter equal to the core diameter of the rods, i.e. 15 mm. All specimens were conditioned to standard temperature and relative humidity conditions (20°C / 65% R.H.), leading to approximately 12% moisture content in the wood.

Specimens with two configurations with respect to the edge distances and spacings were tested as shown in Fig. 3e. In configuration A the rods were installed with spacing $a_2 = 2d$ and edge distance $a_{2.CG} = 2.5d$. In configuration B the rods were installed with spacing $a_2 = 4d$ and edge distance $a_{2.CG} = 1.5d$. These specific values were chosen so that the minimum net distance between the rods (in configuration A) or the minimum net distance between the rod and the edge (in configuration B) were equal to the diameter of the rods. The embedment length of the rods in all specimens was l = 450 mm. Specimens with 4 different rod-to-grain angles were tested (α = 15, 30, 60, 90°). Two tests were performed for each configuration and rod-to-grain angle resulting in a total number of 16 tests. The specimens are denoted *Sα-configuration-no* based on their rod-to-grain angle α, their configuration (A or B) and the serial number of the test. Testing was performed using the loading protocol given in EN 26891:1991 (ISO6891:1983) (CEN 1991). The test program is summarized in Table 2.

Table 2: Test program

Specimen Series	$b \times h \times L$ (mm)	ρ_m [a] (kg/m^3)	α (deg)	l (mm)	d / d_c (mm)	a_2 (mm)	$a_{2.CG}$ (mm)
S15-A-(1-2)	140×545×1200	481.3	15	450	20 / 15	40	50
S15-B-(1-2)	140×545×1200	481.3	15	450	20 / 15	80	30
S30-A-(1-2)	140×545×940	482.2	30	450	20 / 15	40	50
S30-B-(1-2)	140×545×940	482.6	30	450	20 / 15	80	30
S60-A-(1-2)	140×545×765	469.6	60	450	20 / 15	40	50
S60-B-(1-2)	140×545×765	485.5	60	450	20 / 15	80	30
S90-A-(1-2)	140×545×500	472.6	90	450	20 / 15	40	50
S90-B-(1-2)	140×545×500	476.5	90	450	20 / 15	80	30

[a] Determined for the whole specimen

2.2 ANALYTICAL

Analytical expressions for withdrawal capacity, stiffness and the stress and displacement distributions of single rods can be found in (Stamatopoulos and Malo 2015b; Stamatopoulos and Malo 2016). This model is based on classical Volkersen theory (Volkersen 1938) applied to axially loaded fasteners (Jensen et al. 2001). It is assumed that all shear deformation, $\delta(x)$, occurs in a shear zone of finite dimensions and it is related to the mean interfacial shear stress, $\tau(x)$, by a bi-linear constitutive $\tau(x)$- $\delta(x)$ relationship. An example of a real non-linear behaviour is compared to the modelled bi-linear relationship in Fig. 4. The bi-linear idealization separates the curve in two distinct domains; the linear elastic domain and the fracture domain. These domains are characterized by the equivalent shear stiffness parameters Γ_e and Γ_f, which are the slopes of the two branches of the bi-linear constitutive relationship.

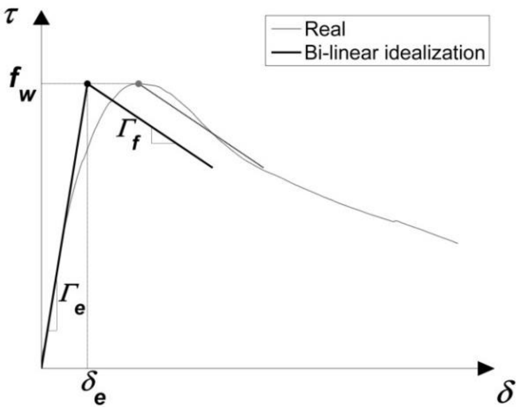

Fig. 4 Real and idealized bi-linear $\tau(x)$-$\delta(x)$ curve

The model can be extended to a group of multiple rods symmetrically installed 'in parallel' under the assumption that Γ_e and Γ_f, are the same for all rods. For the pull-push or the pull-shear loading condition, the withdrawal stiffness, K_w, is equal to:

$$K_w = n_{ef.ser} \cdot \pi \cdot d \cdot l_{ef} \cdot \Gamma_e \cdot \frac{\tanh\omega_n}{\omega_n} \tag{3}$$

The effective number of rods for the serviceability limit state, $n_{ef.ser}$, is used in order to take into account possible group effects and its value is discussed in Section 3.2.

The withdrawal capacity, $P_{u.w}$, is given by Eq. (4):

$$\frac{P_{u.w}}{\pi \cdot d \cdot l_{ef} \cdot f_w} = n_{ef} \cdot \left(\frac{\sin(m \cdot \omega_n \cdot \lambda_u)}{\omega_n \cdot m} + \frac{\tanh[\omega_n \cdot (1\text{-}\lambda_u)] \cdot \cos(m \cdot \omega_n \cdot \lambda_u)}{\omega_n} \right) \approx n_{ef} \cdot P_{u.w.single} \tag{4}$$

where f_w is the withdrawal strength and $m = \sqrt{\Gamma_f / \Gamma_e}$ is a parameter which expresses the brittleness of the shear zone. Note that n_{ef} has been used in Eq. (4) in order to take into account possible group effect on capacity of multiple rods, and its value is discussed in Section 3.1.

The parameter ω_n is defined as:

$$\omega_n = \sqrt{\pi \cdot d \cdot \Gamma_e \cdot \beta_n \cdot l_{ef}{}^2} \tag{5}$$

where β_n is given by:

$$\beta_n = \frac{1}{A_s \cdot E_s} + \frac{n}{A_w \cdot E_{w.\alpha}} \tag{6}$$

Here E_s and $E_{w.\alpha}$ are the moduli of elasticity of steel and wood (as function of α), respectively. The core cross-sectional area of the rod is $A_s = \pi \cdot d_c^2/4$ and A_w is the area of wood subjected to axial stress. $E_{w.\alpha}$ may be estimated by the Hankinson formula and A_w by an effective area, confer (Stamatopoulos and Malo 2016).

The effective length l_{ef} and the parameters Γ_e (in N/mm³), f_w (in MPa) and m and are given by Equations (7)-(10) (Stamatopoulos 2016):

$$l_{ef} = l - 0.5 \cdot d \tag{7}$$

$$\Gamma_{e.\alpha} = \frac{9.65}{1.5 \cdot \sin^{2.2}\alpha + \cos^{2.2}\alpha} \tag{8}$$

$$f_{w.\alpha} = \frac{4.70}{0.95 \cdot \sin^{2.2}\alpha + \cos^{2.2}\alpha} \tag{9}$$

$$m_\alpha = \frac{0.332}{1.73 \cdot \sin\alpha + \cos\alpha} \tag{10}$$

Note that, in principle, the parameters Γ_e and Γ_f for withdrawal of multiple rods are different from the single rod case due to stresses' interaction. However, for rods installed 'in parallel' the difference is assumed to be small. For rods installed in small angles to the grain there is a high shear stress concentration in the vicinity of the interface (i.e. the magnitude of shear stresses is much higher near the interface). For rods installed with greater angles to the grain, the shear stress distributes mainly along the strong shear plane. Therefore, Eq. (8) is assumed to be a good approximation. Possible group effects may indirectly be taken into account by the use of $n_{ef.ser}$ in Eq. (3). Note that such an approach will provide the same estimation for a given angle, regardless of the configuration of rods with respect to edge distances and spacings. The parameter λ_u is a dimensionless length parameter which expresses the percentage of the embedment length at failure in which fracture behaviour takes place and it can be determined by the diagram given in Fig. 5.

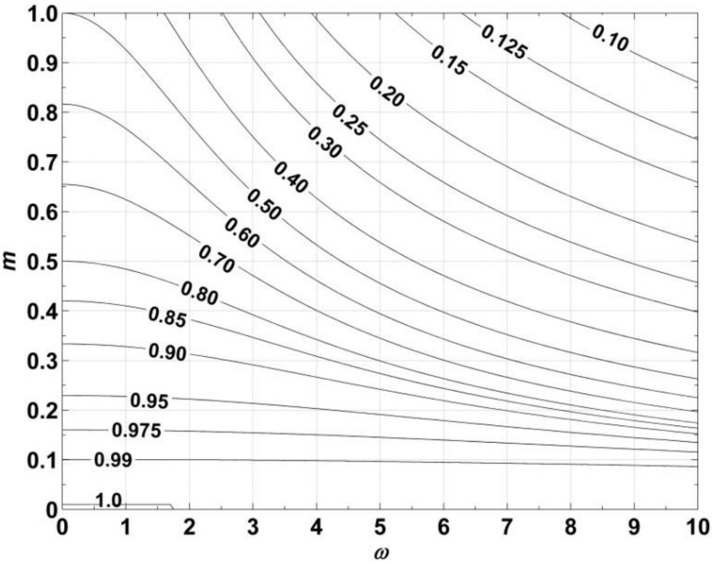

Fig. 5 Diagram for the determination of λ_u (Stamatopoulos and Malo 2015b)

2.3 NUMERICAL

Finite element simulations were performed to estimate the withdrawal stiffness as well as the stress and displacement distributions in all specimens. Abaqus software (Abaqus analysis user's guide, Version 6.13 2013) was used for the finite element simulations. The finite element model assembly is visualized in Fig. 6a. It consists of a rectangular box-type timber part in surface contact with the embedded threaded rods. The threads and the core of the threaded rod were meshed independently in separate sub-parts, which were jointed using a tie constrain as shown in Fig. 6b. Similarly, the timber part was created by tying two independently meshed sub-parts; a sub-part with the respective female thread geometry of the rod and an exterior timber sub-part. These two parts were tied in the interface between the timber part and the outer thread surface of the rod; confer the detail shown in Fig. 6c. The timber part was more densely meshed in the vicinity of the interface with the threaded rod. The mesh size gradually increased with increasing distance from the interface. Three dimensional, 8-node, linear brick elements were used to mesh all parts. Each threaded rod was loaded by a unit vertical pull-out force, P = 1 kN. Lateral displacements of the rods at the loading point were restrained.

Wood is an anisotropic material, which can be approximated as orthotropic with three distinct material orientations; the longitudinal (parallel to the grain), the radial and the tangential (with respect to the annular rings). The subscripts L, R and T are used to indicate these material directions. However, in these simulations wood was modelled as transversely isotropic (in Cartesian coordinates), assuming equal properties in the radial and the tangential directions. The material properties given in Table 3 were used for the simulations. Due to an incomplete set of material properties provided by the manufacturer, the lacking properties were taken from a study on mechanical properties of Norwegian spruce (Dahl 2009). The steel of the rods was modelled as isotropic with modulus of elasticity equal to E_s= 210 GPa and Poisson's ratio equal to 0.30. Both steel and wood were modelled as linear-elastic. The contact interaction between the wood and the rod was modelled with hard contact normally to the surface and frictional behaviour tangentially. For the normal contact, the augmented Lagrange method was used as constraint enforcement method. The friction coefficient for the wood-steel surface was set equal to μ= 0.20. This decision was supported by the study of (Koubek and Dedicova 2014) who investigated the friction coefficient of wood products (laminated veneer lumber and pine wood) as function - among others - of the angle to the grain and contact pressure. This study showed that for normal moisture content and pressure parallel to the grain, the friction coefficient is approximately equal to 0.25 and 0.20 for low and high values of the contact pressure, respectively. For other angles, the friction coefficient was found to be smaller. Depending on the specimen the friction coefficient was in the range of 0.15-0.30 for low contact pressure and in the range of 0.12-0.22 for higher contact pressure. The numerical results for varying friction coefficient in these ranges are very similar and therefore a constant value of μ= 0.20 was assumed to be a reasonable input value for the Finite Element simulations.

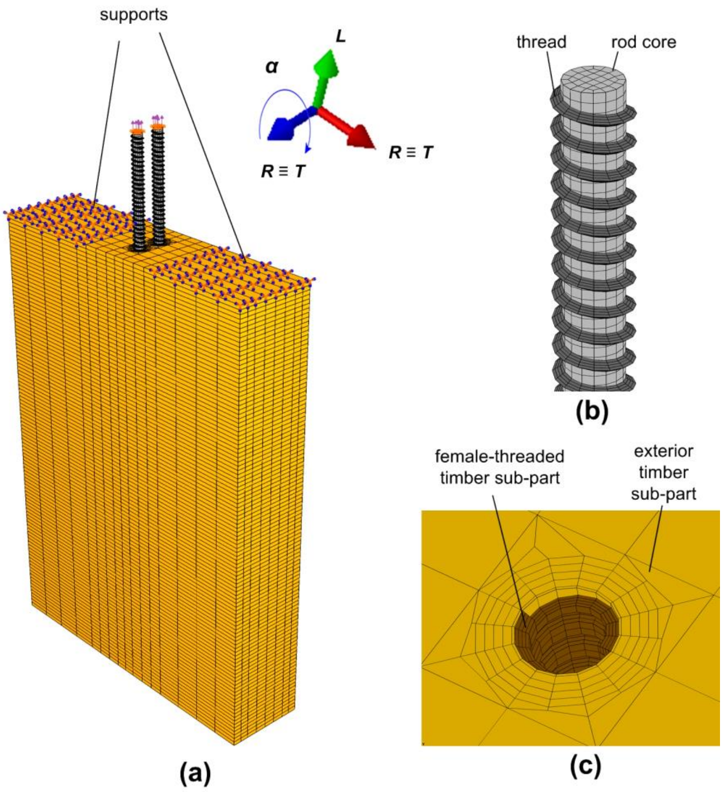

Fig. 6 Numerical simulation: (a) model assembly (b) finite element model of the threaded rod, and (c) detail of the finite element model of the timber part

Table 3: Material properties for numerical simulation

Material property	Symbol	Value	Input for Simulation
Mean density (kg/m^3)	ρ_m	470 [a]	470
Moduli of Elasticity (MPa)	$E_L \equiv E_{w.0}$	13000 [a]	13000
	$E_R = E_T \equiv E_{w.90}$	410 [a]	410
Shear Moduli (MPa)	$G_{LR} = G_{LT}$	760 [a]	760
	G_{RT}	30.7 [b]	30
Poisson ratios	ν_{LR}	0.501 [b]	0.60
	ν_{LT}	0.695 [b]	
	ν_{TR}	0.315 [b]	0.60
	ν_{RT}	0.835 [b]	

[a] Values provided by the manufacturer

[b] Values by (Dahl 2009)

3 RESULTS AND DISCUSSION

3.1 WITHDRAWAL CAPACITY

All specimens failed due to withdrawal of the rods. Typical failure modes for each specimen series are depicted in Fig. 7. For specimens with α ≠ 90° a splitting crack formed along the grain, confer the photos (a)-(f) in Fig. 7.

However, this crack was bridged by the rods and did not appear to have a strong influence on the structural behaviour.

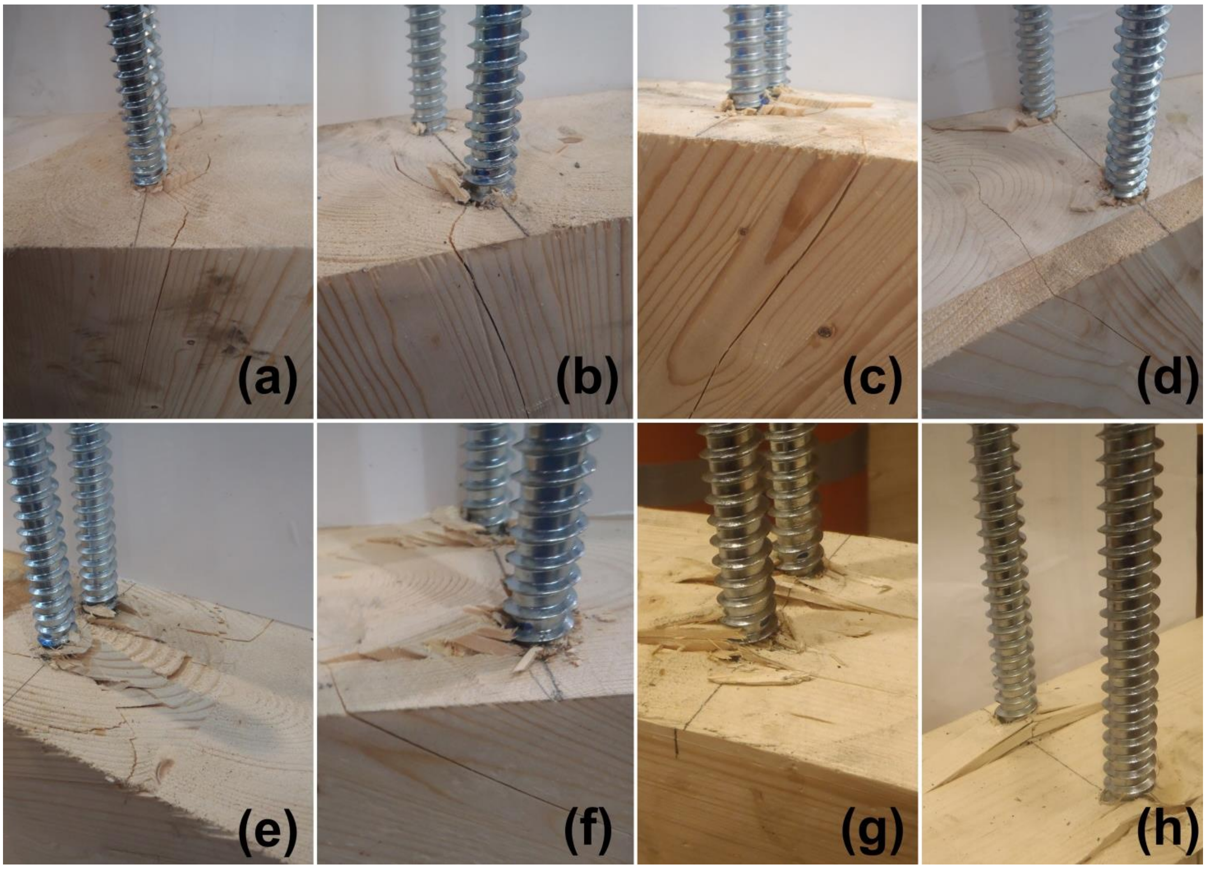

Fig. 7 Typical failure modes of series (a) S15-A, (b) S15-B, (c) S30-A, (d) S30-B, (e) S60-A, (f) S60-B, (g) S90-A and (h) S90-B

The experimental results for the withdrawal capacity are summarized in Table 4. The withdrawal capacity for each specimen and the mean capacity for each configuration and angle are provided. Treating all experimental results for the withdrawal capacity as one sample, a coefficient of variation (abbr. CoV) equal to 5.3% is obtained. This value of CoV is quite similar to the case of single rods if small values of α-which are inherently variable-are excluded (for example by use of the experimental results of the reference single rods study (Stamatopoulos and Malo 2015b) we obtain CoV= 8.8% if results for α= 0° are excluded and CoV= 6.2% if results for α= 0°, 10° are excluded for rods with l= 450 mm). Thus the capacity is quite reliable and its variability is similar to the reliability in the case of single rods and therefore approximate conclusions can be obtained despite the small sample size.

For specimens with α= 60°, 90° the mean withdrawal capacity of specimens with the configuration A was greater by 0.9% and 0.4% respectively, compared to specimens with the configuration B. For specimens with α= 30°, the experimentally recorded mean withdrawal capacity was greater for configuration B by 4.5% compared to configuration A. One recording was lost for a specimen with α= 15° and rods installed in the configuration B, and thus a reasonable comparison between the configurations for α= 15° is not possible. As seen by the results in Table 4 the withdrawal capacity is characterized by very small variability.

Characteristic values for the withdrawal capacity were also calculated by considering all results per angle as one sample, i.e. without distinguishing between different configurations. CoV was very small for all samples (7% for α= 15°, 3% for α= 30 and 60°, and 1% for α= 90°). The characteristic values were determined in accordance with EN 14358 (CEN 2006) and they are also provided in Table 4. EN 14358 (CEN 2006) assumes that the test values are log-normally distributed. Despite the small size of each sample the calculated characteristic withdrawal capacities are assumed to be a reasonable approximation, due to the use of a minimum value of 0.05 for the standard deviation of the natural logarithms of test values, according to EN 14358 (CEN 2006) in cases where CoV is smaller than 5%.

The effective numbers of rods n_{ef} (both for mean and characteristic values) are also given in Table 4. They were determined by use of results from the reference single rod experimental investigation of specimens with the same threaded rods and the same glulam strength class as in the present investigation (Stamatopoulos and Malo 2015a; 2015b). The individual and mean values of n_{ef} are plotted as function of α in Fig. 8. Based on the obtained mean-level experimental results the following approximating expression was derived for n_{ef}:

$$n_{ef} = \begin{cases} 1.75 + 0.116 \cdot (\alpha / 60°) \,, & \alpha < 60° \\ n^{0.9} = 1.866 \,, & \alpha \geq 60° \end{cases} \tag{11}$$

The analytical estimations (also provided in Table 4) were made according to Eq. (4), using the effective number of rods provided by Eq. (11). The experimental results together with analytical estimation are plotted as function of α in Fig. 9. As shown in these figures they are in good agreement with the analytical estimations being slightly conservative.

Table 4: Results-withdrawal capacity $P_{u.w}$ (kN)

Specimen series	**Experimental**				**Analytical mean** [a]
	Test 1	Test 2	Mean (n_{ef} [b])	Characteristic (n_{ef} [c])	
S15-A-(1-2)	247.5	223.5	235.5 (1.72)	191.5 (1.79)	228.6
S15-B-(1-2)	258.9	(-) [d]	258.9 (1.89)		
S30-A-(1-2)	250.1	260.3	255.2 (1.77)	226.7 (1.96)	243.4
S30-B-(1-2)	265.6	267.8	266.7 (1.84)		
S60-A-(1-2)	277.8	271.4	274.6 (1.94)	237.5 (1.90)	257.9
S60-B-(1-2)	283.0	261.5	272.2 (1.92)		
S90-A-(1-2)	259.0	263.7	261.4 (1.88)	226.7 (1.86)	243.7
S90-B-(1-2)	261.3	259.5	260.4 (1.87)		

[a] Values for analytical approach (Stamatopoulos and Malo 2016):
$E_{w.0}$ =13000 MPa, $E_{w.90}$ =410 MPa, $E_{w.\alpha} = E_{w.0} \cdot E_{w.90} / (E_{w.0} \cdot \sin^2\alpha + E_{w.90} \cdot \cos^2\alpha)$, E_s = 210000 MPa
$A_w \equiv A_{w.eff} = 2 \cdot 140 \cdot (180 + 450/6) = 71400$ mm^2 , $A_s = \pi \cdot d_c^2 /4 = 176.6$ mm^2

[b] Mean experimentally recorded capacities of specimens with single rods (Stamatopoulos and Malo 2015b):
$P_{u.w.15}$ = 136.7 kN (mean of $P_{u.w.10}$ and $P_{u.w.20}$), $P_{u.w.30}$ = 144.6 kN, $P_{u.w.60}$ = 141.7 kN, $P_{u.w.90}$ = 139.2 kN

[c] Characteristic experimentally recorded capacities of specimens with single rods (Stamatopoulos and Malo 2015a):
$P_{u.w.15.k}$ = 106.7 kN (mean of $P_{u.w.10.k}$ and $P_{u.w.20.k}$), $P_{u.w.30.k}$ = 115.5 kN, $P_{u.w.60.k}$ = 125.2 kN, $P_{u.w.90.k}$ = 121.9 kN

[d] Recording was lost

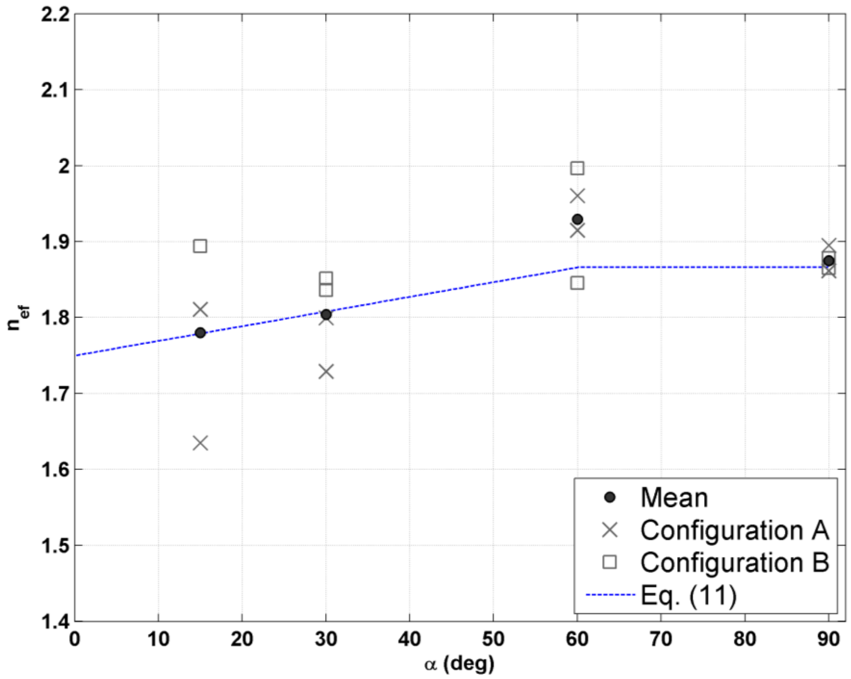

Fig. 8 Experimentally determined values of n_{ef} as function of α

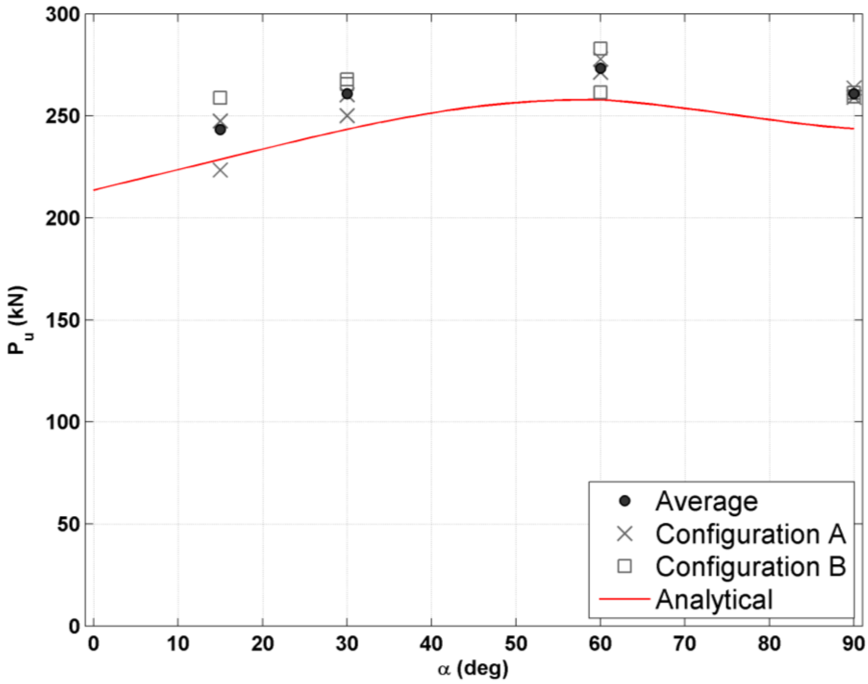

Fig. 9 Withdrawal capacity as function of α

3.2 WITHDRAWAL STIFFNESS

The experimental results for the withdrawal stiffness together with the analytical and the numerical estimations are summarized in Table 5 and plotted as function of α in Fig. 10. The specimens exhibited very high withdrawal stiffness especially for small angles. Note that only a small number of tests have been performed and hence the measured values for stiffness may not be representative in general. Analytical estimations were made according to Eq. (3) assuming two different effective number of rods; the actual number of rods ($n_{ef.ser}$= 2) and the effective number of rods given by Eq. (2). In general, $n_{ef.ser}$= 2 provided a better analytical estimation than Eq. (2). The agreement between experimental results and the analytical and numerical estimations is very good. According to the experimental results, the difference between the values for configurations A and B was relatively small (configuration B was stiffer by 7.1%, 14.6% and 1.4% for α= 15°, 30° and 90° respectively while configuration A was stiffer by 5.3% for α= 60°) . The distributions of stresses and displacements along the rod were quantified by the numerical simulations. These distributions were essentially the same as the distributions for the single rod case (Stamatopoulos and Malo 2016) and therefore they are not presented in the present paper.

Table 5: Results-withdrawal stiffness K_w (kN/mm)

Specimen series	**Experimental**			**Analytical** [a]		**Numerical**
	Test 1	Test 2	Mean	$n_{ef.ser}$ = 2	$n_{ef.ser}$ = $2^{0.8}$	
S15-A-(1-2)	299.7	220.6	260.2	258.5	225.0	273.7
S15-B-(1-2)	318.3	237.8	278.0			281.1
S30-A-(1-2)	170.4	226.3	198.3	219.5	191.1	233.6
S30-B-(1-2)	184.5	270.0	227.3			239.9
S60-A-(1-2)	118.1	149.3	133.7	151.8	132.5	151.6
S60-B-(1-2)	131.3	122.5	126.9			157.2
S90-A-(1-2)	144.8	108.8	126.8	129.2	112.5	127.4
S90-B-(1-2)	139.1	118.0	128.6			132.5

[a] Values for analytical approach: same as in Table 4

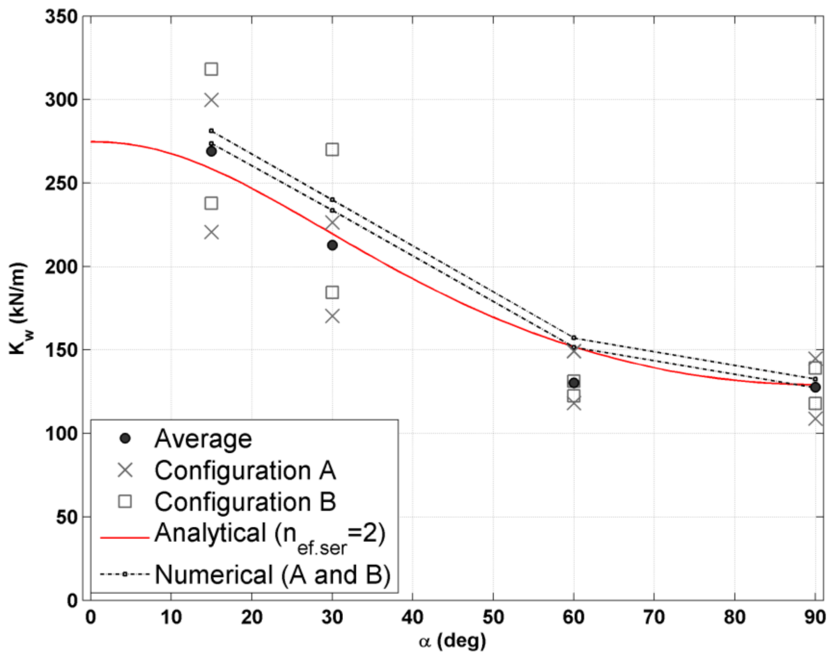

Fig. 10 Withdrawal stiffness as function of α

4 CONCLUSIONS

The withdrawal of pairs of axially loaded threaded rods screwed into glued-laminated timber elements was studied. The rods were installed in ‘parallel’, i.e. in a row perpendicular to the plane of the grain. Specimens with two configurations with respect to the edge distances and spacings were tested; one with small spacing between the rods (configuration A) and one with small edge distances (configuration B). The edge distances and spacings were smaller than the minimum values required by EC5 (CEN 2004). The outer thread diameter and the embedment length of the threaded rods were d= 20 mm and l= 450 mm, respectively. Specimens with 4 different rod-to-grain angles were tested (α= 15, 30, 60, 90°). Analytical and numerical estimations were compared to the experimental results. The following main conclusions are drawn:

- Interaction effects (group effect) of the rods were approximated by use of an effective number of rods n_{ef}.
- The values of n_{ef}, were evaluated on the basis of experimental results and a simple approximating expression for its determination was derived. Despite very small edge distances and spacings the mean values of n_{ef} per configuration and angle were in the range 1.72-1.94.
- Based on the obtained experimental results, the difference between the results for configurations A and B was-in general-small.
- The withdrawal capacity and stiffness can be estimated by an analytical model which is based on Volkersen model with an idealized bi-linear constitutive relationship.
- The withdrawal stiffness can be estimated with sufficient accuracy by finite element simulation.

ACKNOWLEDGEMENTS

The support by The Research Council of Norway (208052) and The Association of Norwegian Glulam Producers, Skogtiltaksfondet and the Norwegian Public Road Administration is gratefully acknowledged.

REFERENCES

Abaqus analysis user's guide, Version 6.13 (2013). Dassault Systèmes Simulia corp.,

Angst V, Malo KA (2012) The effect of climate variations on glulam-An experimental study European Journal of Wood and Wood Products 70:603-613 doi:10.1007/s00107-012-0594-y

Blaß HJ, Krüger O (2010) Schubverstärkung von Holz mit Holzschrauben und Gewindestangen. KIT Scientific Publishing, Karlsruhe

Blaß HJ, Laskewitz B (1999) Effect of spacing and edge distance on the axial strength of glued-in rods. Paper presented at the Proceedings of the 32nd CIB-W18 meeting Graz, Austria,

Carradine D, Newcombe P, Buchanan A (2009) Using screws for structural applications in laminated veneer lumber. Paper presented at the Proceedings of the 42nd CIB-W18 meeting Dübendorf, Switzerland,

CEN, European committee for standardization (1991) EN 26891:1991 (ISO 6891:1983): Timber structures-Joints made with mechanical fasteners-General principles for the determination of strength and deformation characteristics. Brussels, Belgium

CEN, European committee for standardization (2004) EN 1995-1-1:2004: Design of timber structures. Part 1-1: General-Common rules and rules for buildings. Brussels, Belgium

CEN, European committee for standardization (2006) EN 14358-2006: Timber structures- Calculation of characteristic 5-percentile values and acceptance criteria of a sample. Brussels, Belgium

CEN, European committee for standardization (2013) EN 14080-2013: Timber structures- Glued laminated timber and glued solid timber - Requirements. Brussels, Belgium

Dahl K (2009) Mechanical properties of clear wood from Norway spruce. Ph.D. Thesis, Norwegian University of Science and Technology

DIBt, Deutsches Institut für Bautechnik (2010) SFS intec, GmbH., Gewindestangen mit Holzgewinde als Holzverbindungsmittel, Allgemeine bauaufsichtliche Zulassung Z-9.1-777.

DIBt, Deutsches Institut für Bautechnik (2011) SFS intec, GmbH., SFS Befestiger WT-S-6,5; WT-T-6,5; WT-T-8,2; WR-T-9,0 und WR-T-13 als Holzverbindungsmittel, Zulassungnummer Z-9.1-472.

DIBt, Deutsches Institut für Bautechnik (2013) European Technical Approval ETA-11/0190.

DIN, Deutsches Institut für Normung. (2008) DIN 1052:2008-12: Design of timber structures-General rules and rules for buildings. Berlin, Germany

Gehri E (2009) Influence of fasteners spacings on joint performance - Experimental results and codification. Paper presented at the Proceedings of the 42nd CIB-W18 meeting Dübendorf, Switzerland,

Jensen JL, Koizumi A, Sasaki T, Tamura Y, Iijima Y (2001) Axially loaded glued-in hardwood dowels Wood Science and Technology 35:73-83

Koubek R, Dedicova K (2014) Friction of wood on steel. Master's Thesis, Linnaeus University

Krenn H, Schickhofer G (2009) Joints with inclined screws and steel plates as outer members. Paper presented at the Proceedings of the 42nd CIB-W18 meeting Dübendorf, Switzerland,

Mahlknecht U, Brandner R, Ringhofer A, Schickhofer G (2014) Resistance and Failure Modes of Axially Loaded Groups of Screws. In: Aicher S, Reinhardt HW, Garrecht H (eds) Materials and Joints in Timber Structures -Recent Developments of Technology, vol 9. Springer: RILEM Bookseries, pp 289-300. doi:10.1007/978-94-007-7811-5_27

Mori T, Nakatani M, Kawahara S, Shimizu T, Komatsu K (2008) Influence of the number of fastener on tensile strength of lagscrewbolted glulam joint. Paper presented at the Proceedings of the 10th World Conference on Timber Engineering, Miyazaki, Japan,

Nakatani M, Komatsu K (2004) Development and verification of theory on pull-out properties of Lagscrewbolted timber joints. Paper presented at the Proceedings of the 8th World Conference on Timber Engineering, Lahti, Finland,

Nakatani M, Walford B (2010) Influence of timber dimension on withdrawal behaviour of lagscrewbolt. Paper presented at the Proceedings of WCTE 2010 - World Conference on Timber Engineering, Trentino, Italy,

Ringhofer A, Brandner R, Schickhofer G (2015) A universal approach for withdrawal properties of self-tapping-screws in solid timber and laminated timber products. Paper presented at the Proceedings of the 2nd INTER meeting Šibenik, Croatia,

Stamatopoulos H (2016) Withdrawal properties of threaded rods embedded in glued-laminated timber elements. Ph.D. Thesis, Norwegian University of Science and Technology

Stamatopoulos H, Malo KA (2015a) Characteristic withdrawal capacity and stiffness of threaded rods. Paper presented at the Proceedings of the 2nd INTER meeting Šibenik, Croatia,

Stamatopoulos H, Malo KA (2015b) Withdrawal capacity of threaded rods embedded in timber elements Construction and Building Materials 94:387-397 doi:http://dx.doi.org/10.1016/j.conbuildmat.2015.07.067

Stamatopoulos H, Malo KA (2016) Withdrawal stiffness of threaded rods embedded in timber elements Construction and Building Materials 116:263-272 doi:http://dx.doi.org/10.1016/j.conbuildmat.2016.04.144

Volkersen O (1938) Die nietkraftverteilung in zugbeanspruchten nietverbindungen mit konstanten laschenquerschnitten Luftfahrtforschung 15:41-47